Interplay of Peltier and Seebeck Effects in Nanoscale Nonlocal Spin Valves

F. L. Bakker,* A. Slachter, J.-P. Adam, and B. J. van Wees

Physics of Nanodevices, Zernike Institute for Advanced Materials, University of Groningen, The Netherlands
(Received 31 March 2010; published 24 September 2010)

We have experimentally studied the role of thermoelectric effects in nanoscale nonlocal spin valve devices. A finite element thermoelectric model is developed to calculate the generated Seebeck voltages due to Peltier and Joule heating in the devices. By measuring the first, second, and third harmonic voltage response nonlocally, the model is experimentally examined. The results indicate that the combination of Peltier and Seebeck effects contributes significantly to the nonlocal baseline resistance. Moreover, we found that the second and third harmonic response signals can be attributed to Joule heating and temperature dependencies of both the Seebeck coefficient and resistivity.

The Seebeck and the related Peltier effects are the fundamental phenomena of thermoelectricity, a field subject to extensive research during the previous decades [1]. Although these are bulk material properties, they can be utilized to measure the temperature or to generate heat locally at or close to an interface between different materials. While progress in nanoscale device fabrication has made it possible to study these phenomena at continuously decreasing length scales, they are rarely taken into account to analyze electrical measurements in nanostructures. In the specific field of spintronics, a detailed understanding of the interaction between heat transport and the charge and spin degrees of freedom is highly required [2]. This emerging branch, called *spin caloritronics* [3], has recently drawn considerable attention [4–8], and (spin-) thermoelectric effects have been experimentally examined in magnetic multilayer nanostructures [6,7] and in macroscopically large ferromagnetic strips [8]. In this Letter, we use lateral nonlocal spin valve devices as a tool to study the interplay between heat, charge and spin at the nanoscale. The nonlocal device design enables us to separate the charge and heat current, and hence, excludes spurious effects. We find that the baseline resistance in nonlocal spin valve measurements originates mainly from Peltier heating or cooling at the injector junction and the Seebeck effect at the detector junction. Furthermore, we demonstrate that it is experimentally feasible to use basic thermoelectrics to obtain control over the heat flow in nanostructures.

The nonlocal spin valve experiment is schematically depicted in Fig. 1(a). Two Permalloy (Py) electrodes are overlapped with a Cu strip, creating two ferromagnetic-nonmagnetic metal (F-N) interfaces. Electrical spin injection across a F-N interface is well-described in terms of a two-current model [9,10] and was demonstrated experimentally [11,12]. Here, a spin current is injected into the Cu strip by sending a charge current through the first F-N interface [Fig. 1(a)]. A spin voltage can be detected at the second interface provided that the spacing between

injector and detector is shorter than the spin relaxation length of the Cu [12].

Ideally, the voltage detected at the second interface in the nonlocal geometry will be zero in the absence of a spin accumulation. Since the current and voltage path are completely separated, one expects no Ohmic voltage drop at interface 2 [Fig. 1(a)]. The voltage arising from a spin accumulation is bipolar, having equal magnitude but opposite sign for the parallel and antiparallel alignment of both ferromagnets. However, the baseline resistance observed in experiments, defined as the resistance in the absence of spin-related effects, is in general nonzero [12]. Current spreading at the injector can account for an Ohmic resistance at the detector, as discussed by Johnson and Silsbee [13]. The resulting voltage V_r is found to depend exponentially on the separation L between the two interfaces as $V_r \propto e^{-\pi L/W}$, with W the width of the Cu strip. Moreover, spin-dependent scattering at the detector interface [14] has been invoked to explain an offset voltage, but both effects are not sufficient to describe the data accurately.
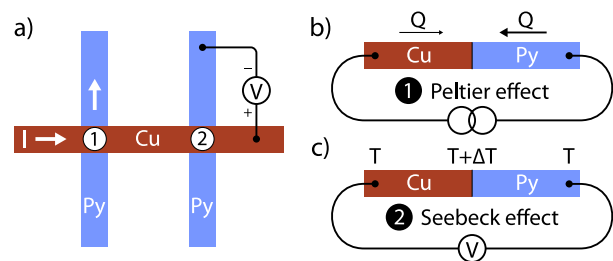

FIG. 1 (color online).   (a) Schematic drawing of a typical spin valve experiment. Current is sent through the first Cu/Py interface, while the voltage drop is measured at the second interface. (b) Because of the difference in the Peltier coefficients for Cu and Py, the heat current Q carried by the electrons changes across the interface. Hence, interface 1 is locally heated or cooled depending on the direction of the current. (c) The second interface acts as a thermocouple and detects the local electron temperature via the Seebeck effect.

Here we address a new origin of the baseline resistance, composed of thermoelectric phenomena which are generally disregarded in the analysis. We show that the Peltier and the related Seebeck effect, when combined in a lateral nanostructure, give rise to a significant modification of the baseline resistance.

If an electrical current I flows through a Cu/Py interface, heat accumulates or is absorbed at the interface due to the mismatch of the Peltier coefficients. The heat current carried by the electrons, represented by the Peltier coefficient, is different on both sides of the interface. Since the charge current is continuous across the interface, the heat current has a discontinuity. Consequently, the interface is heated or cooled depending on the sign of the current [Fig. 1(b)]. The inverse process, called the Seebeck effect, refers to the generation of a voltage by a temperature gradient. This effect can be exploited to probe the local electron temperature at or close to the interface, similar to the functioning of a thermocouple [Fig. 1(c)]. As copper is an excellent thermal conductor, the heat generated at interface 1 can be efficiently transferred to interface 2 and is then, via the Seebeck effect, translated back into a voltage.

In order to quantify the Peltier and Seebeck effects a 3D thermoelectric finite element model (FEM) is developed. The charge current density J and the heat current density Q in these nanostructures can be related to the voltage and temperature in the following way:

$$\begin{pmatrix} \vec{J} \\ \vec{Q} \end{pmatrix} = -\begin{pmatrix} \sigma & \sigma S \\ \sigma \Pi & \kappa \end{pmatrix} \begin{pmatrix} \vec{\nabla} V \\ \vec{\nabla} T \end{pmatrix} \qquad (1)$$

with σ the electrical conductivity, κ the thermal conductivity, S the Seebeck coefficient, and $\Pi = S T_0$ the Peltier coefficient. T_0 is the reference temperature of the device and taken to be 300 K. The charge and heat currents are taken to be continuous across the boundaries and at the end of all contacts we set the temperature at T_0. Joule heating and charge conservation is incorporated via $\nabla Q = J^2/\sigma$ and $\nabla J = 0$. We use a separate two-current model to calculate the spin signals by introducing spin-dependent conductivities $J_{\uparrow,\downarrow} = -\sigma_{\uparrow,\downarrow}/e \nabla \mu_{\uparrow,\downarrow}$, with $\sigma_{\uparrow,\downarrow}$ and $\mu_{\uparrow,\downarrow}$ the spin-dependent conductivity and electrochemical potential, respectively [9,10,15]. Bulk spin relaxation is introduced via $\nabla J_{\uparrow,\downarrow} = \mp \frac{(1-P^2)\sigma}{4e\lambda^2}(\mu_\uparrow - \mu_\downarrow)$, with λ the spin relaxation length and P the conductivity polarization given by $\frac{\sigma_\uparrow - \sigma_\downarrow}{\sigma_\uparrow + \sigma_\downarrow}$.

Two batches of lateral nonlocal spin valve devices were fabricated on a thermally oxidized Si substrate in a five-step e-beam lithography process. Figure 2 shows the scanning electron microscope (SEM) images of the two types of devices. A device consists of two 15 nm thick Py islands, a large injector FM$_1$ (1 μm × 300 nm) and a small detector FM$_2$ (150 nm × 50 nm), separated from each other by a distance L. Both ferromagnets are contacted on one side with Au electrodes and with a 60 nm thick Cu strip on the other side. To reduce Joule heating in the leads, the Au contacts on FM$_1$ have a thickness of 170 nm. The metallic
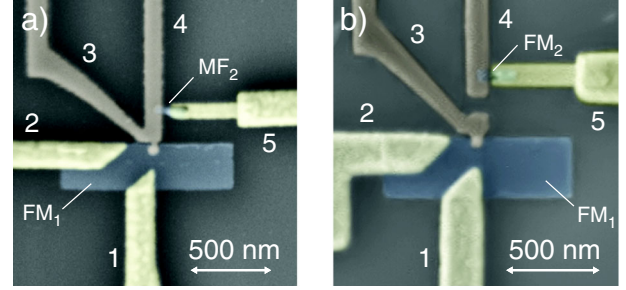

FIG. 2 (color online). Scanning electron microscope (SEM) image of the device layout. (a) Standard nonlocal spin valve geometry. Current is sent from contact 1 to 3, while the voltage is measured between 5 and 4. Contact 2 is not used. (b) Similar device geometry with an electrically isolated detector circuit.

layers are deposited using an e-beam evaporator with a base pressure of 1×10^{-6} mbar. Prior to deposition of Au and Cu the interfaces are cleaned by Ar ion milling to assure good Ohmic interfaces.

We use a lock-in amplifier for detecting the voltage V across the Cu/FM$_2$ interface, between contacts 5 and 4 (Fig. 2). Simultaneously an ac current I is sent from contact 1 to 3. If the response of the system is nonlinear, the higher order terms can be extracted separately by measuring the higher harmonics:

$$V = R_1 I + R_2 I^2 + \dots \qquad (2)$$

with R_i ($i = 1, 2, \dots$) the ith harmonic "resistance" response. The current is applied at a frequency below 1 kHz, much lower than the relevant time scales for thermal conduction in these nanostructures. All electrical measurements are performed at room temperature.

The first harmonic response R_1, reflects the sum of the baseline resistance and a resistance due to the presence of a spin accumulation. The magnetic field dependence of R_1 is shown in Fig. 3(b), with R_{1s} the spin valve signal and R_{1b} defined as the baseline resistance. To examine the distance dependence as proposed by Johnson and Silsbee [13], R_1 is measured for device type 1 [Fig. 2(a)] with different L, varying between 75 and 900 nm. The baseline resistance is plotted in Fig. 3(a). If we neglect thermoelectric effects, the baseline is expected to decrease exponentially as $R_{1b} \propto e^{-\pi L/W}$, with W the width of the Cu contact. The data clearly show an exponential decrease of resistance for small L, but decay more slowly for larger separations. Note that the spin valve voltage shows only an exponential dependence due to spin relaxation in the Cu [shown in Fig. 3(c)]. Assuming that $\lambda_F = 5$ nm for Py, we deduce from our spin-dependent two-current model the spin relaxation length of Cu and bulk conductivity polarization of Py to be 350 nm and 25%, respectively.

For the same set of samples, the magnetic field dependence of the higher harmonic responses R_2 and R_3 is investigated for $L = 200$ nm [shown in Fig. 4(a) and 4(b)]. In addition to a nonzero baseline, we observe a spin voltage in R_2 and R_3 as well. The baseline is measured as a function of
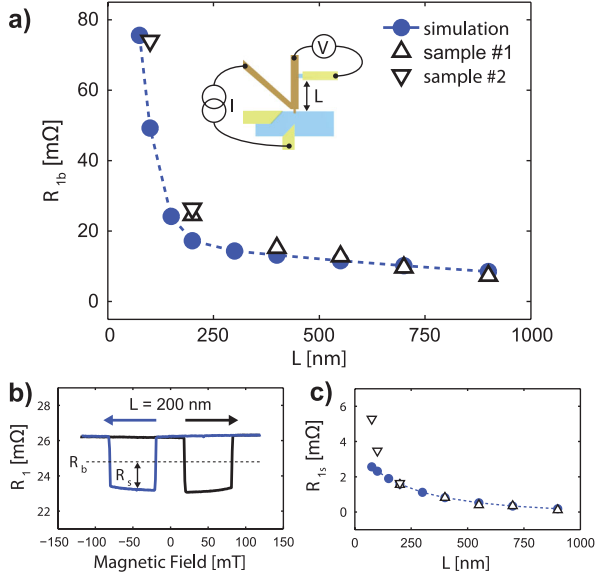
FIG. 3 (color).   (a) R_{1b} measured as a function of the spacing L between the two ferromagnets, as indicated by the measurement geometry in the inset. The triangles reflect measurements taken for two different samples, whereas the blue dots correspond to the FEM calculations. (b) Nonlocal spin valve measurement with the magnetic field swept back and forth, being indicated by the arrows. R_{1s} is defined as the resistance due to the presence of a spin accumulation and R_{1b} is the baseline resistance. (c) R_{1s} as a function of the separation L between both ferromagnets.

the separation L between the two ferromagnets and the result is shown in Figs. 4(c) and 4(d). We find that for R_{2b} the exponential relation to L is absent, whereas R_{3b} shows similar behavior as R_{1b}, decreasing exponentially for

short L and having a much weaker decay for larger separations.

In the following, we show that the observed baselines of R_{1b}, R_{2b} and R_{3b} can be attributed to the Peltier and Seebeck effects. The voltage at the detector can be written as the sum of the spin voltage, a resistive part (V_r) and a Seebeck voltage. For these devices two important sources of heat exist, Peltier heating at the injector interface and Joule heating in the entire current path. Heat is carried away by thermal transport through the metallic leads and via the SiO_2 substrate and consequently, a temperature gradient evolves in the vicinity of FM_2. The generated Seebeck voltage is proportional to a combination of the Seebeck coefficients of Py, Cu, and Au and the temperature gradients in the detector circuit. This circuit can essentially be seen as a thermocouple with an effective Seebeck coefficient S.

In contrast to Peltier heating, being linear with I, Joule heating scales as $\Delta T \propto I^2$. Hence, the thermoelectric contribution to the baseline, $S\Delta T$, originates from Peltier heating for R_1 and from Joule heating for R_2. In order to explain the observed baseline voltage in R_3, we introduce a temperature dependent Seebeck coefficient and resistance. In a linear approximation the temperature dependent Seebeck coefficient is written as $S(T) = S_0(1 + \zeta \Delta T)$, where ΔT the local temperature increase and $\zeta = 1/T_0$ [16]. The resistivity of a metal increases with temperature as $\rho(T) = \rho_0(1 + \alpha \Delta T)$, where α is in the order of 10^{-3} K^{-1} for most metals [17]. Now, R_{3b} refers to the sum of the changes in the Seebeck coefficient and resistance due to Joule heating. Hence, R_{3b} enables us to study these temperature dependencies directly over a small
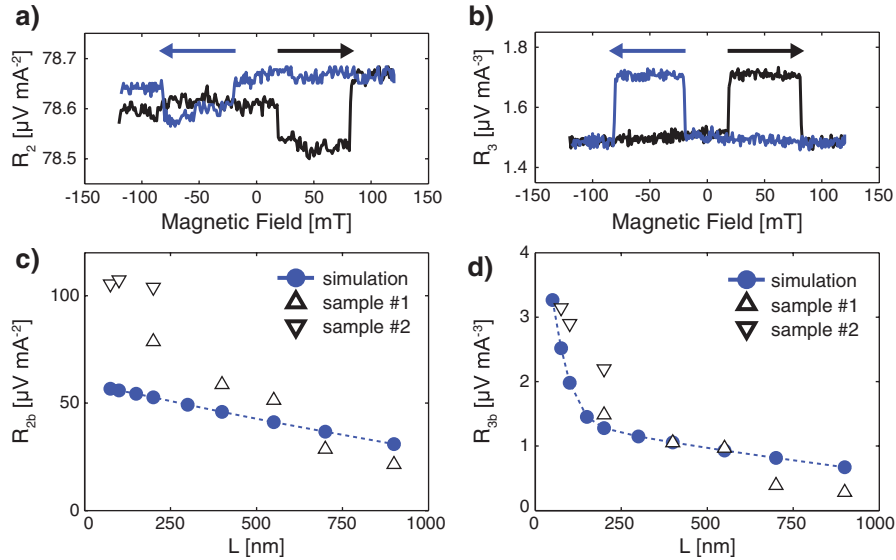

FIG. 4 (color).   (a) R_2 as a function of magnetic field. The baseline resistance is mainly caused by the Seebeck voltage induced by Joule heating. (b) R_3 plotted versus magnetic field. The baseline reflects the modification in Seebeck coefficient and resistance due to temperature changes. Likewise, the spin signal indicates how the spin valve signal is altered by temperature. (c) Baseline resistance R_{2b} as a function of L. Triangles represent data for two different samples, blue dots are simulation results. (d) R_{3b} measured versus L. The shape of R_{3b} is similar to R_{1b} because it describes the temperature dependence of the effects that generate R_{1b}.

TABLE I. Material parameters

Material	σ [S/m]	S [μV/K]	κ [W/mK]
SiO$_2$	10^{-13}	0	1
Au	2.2×10^7	1.7 [17]	300
Cu	4.3×10^7	1.6 [17]	300
Py	4.3×10^6	−20 [8]	30

temperature range of 20 K, the highest achievable temperature raise by Joule heating in our devices. R_{3b} shows similar behavior as R_{1b}, since R_{3b} describes essentially the temperature dependence of R_{1b}. Moreover, R_{2b} is slightly modified by Peltier heating combined with a temperature dependent Seebeck coefficient and resistance. Nevertheless, we do not find an exponential relationship between R_{2b} and L, indicating that the Joule heating induced Seebeck voltage is dominating.

Furthermore, we observe a spin voltage in the higher harmonic responses [shown in Figs. 4(a) and 4(b)]. The spin signal in R_2 can be associated both with the temperature dependence of the spin valve signal (R_{1s}) and with thermally driven spin injection. However, the observed signal has the opposite sign and contradicts with earlier measurements [5,12,14]. The exact origin may be found in the spin-dependent Peltier effect [6] or interface scattering [18]. The spin signal in R_3 reflects the change in the spin valve signal caused by Joule heating. From this measurement, we can derive the spin valve temperature dependence γ, defined as $R_s(T) = R_s(1 - \gamma \Delta T)$. We found a γ of approximately 1%, in good agreement with earlier results [12,14].

The magnitudes of the induced Seebeck voltages have been calculated with the thermoelectric model using Comsol Multiphysics. To obtain the linear response voltage, we have used the parameters presented in Table I [17]. Heat conduction through the substrate is taken into account by assuming a total SiO$_2$ thickness of 1 μm. The model includes both charge and heat currents and reproduces the behavior of R_{1b} remarkably well [Fig. 3(a), blue dots]. For short L, we find an exponential decrease in the baseline resistance, as discussed previously. For larger separations, calculations show that the baseline diminishes more moderately due to thermoelectric effects. We also incorporated the temperature dependence of the resistance and Seebeck coefficient into our thermoelectric model and the simulations are displayed in Figs. 4(c) and 4(d). The slope obtained from the simulation of R_{2b} deviates from the measured data by approximately a factor two. Therefore, we deduce that the Joule heating in the device is 2 times larger than expected. This discrepancy is ascribed to the oxidation of the Py and the interface resistance of the Au contacts, thereby reducing the thermal conduction. For the calculation of R_{3b}, we corrected for this, and obtained a perfect agreement between the simulation of R_{3b} and the experimental data.

To confirm our analysis we excluded charge current effects completely. Therefore, we have measured a similar device with an interrupted Cu strip as shown in Fig. 2(b). Heat conduction can still occur through the SiO$_2$, but charge transport is eliminated. We found a nonzero baseline resistance of 1.85 mΩ for $L = 300$ nm, significantly smaller than without the interruption. This change is mainly due to the difference in thermal conductivity between SiO$_2$ and Cu. FEM calculations predicted a resistance R_{1b} of 1.9 mΩ, in perfect agreement with the observed value. For R_{2b} we found 3.75 μV/mA^2, compared to 4.4 μV/mA^2 for the calculations.

In conclusion, we have demonstrated that thermoelectric effects play an important role in nanoscale spin valve devices and lead to a significant increase in baseline resistance. These effects have been employed to locally raise and probe the electron temperature at the interface of two materials and the experimental results are in good agreement with basic thermoelectric rules. By probing the second and third harmonic response separately, higher order thermal effects are observed. In general, these findings open new possibilities for future caloritronic applications using localized electron temperature control.

*F.L.Bakker@rug.nl

[1] R. D. Barnard, *Thermoelectricity in Metals and Alloys* (Taylor and Francis LTD., London, 1972).
[2] S. O. Valenzuela, Int. J. Mod. Phys. B **23**, 2413 (2009).
[3] G. E. W. Bauer *et al.*, Solid State Commun. **150**, 459 (2010).
[4] Y. Dubi and M. Di Ventra, Phys. Rev. B **79**, 081302(R) (2009).
[5] A. Slachter *et al.*, Nature Phys. (in press).
[6] L. Gravier *et al.*, Phys. Rev. B **73**, 052410 (2006).
[7] Y. Hai-Ming *et al.*, Chin. Phys. Lett. **27**, 027201 (2010).
[8] K. Uchida *et al.*, Nature (London) **455**, 778 (2008).
[9] T. Valet and A. Fert, Phys. Rev. B **48**, 7099 (1993).
[10] P. C. van Son, H. vanKempen, and P. Wyder, Phys. Rev. Lett. **58**, 2271 (1987).
[11] M. Johnson and R. H. Silsbee, Phys. Rev. Lett. **55**, 1790 (1985).
[12] F. J. Jedema *et al.*, Nature (London) **410**, 345 (2001).
[13] M. Johnson and R. H. Silsbee, Phys. Rev. B **76**, 153107 (2007).
[14] S. Garzon, I. Zutic, and R. A. Webb, Phys. Rev. Lett. **94**, 176601 (2005).
[15] L. Gravier *et al.*, Phys. Rev. B **73**, 024419 (2006).
[16] N. F. Mott and H. Jones, *The Theory of the Properties of Metals and Alloys* (Oxford Univ. Press, London, 1936).
[17] C. Kittel, *Introduction to Solid State Physics* (John Wiley & Sons, Inc., New York, 1995), 7th ed..
[18] M. Hatami *et al.*, Phys. Rev. B **79**, 174426 (2009).